Campomelic dysplasia and autosomal sex reversal caused by mutations in an *SRY*-related gene

Jamie W. Foster, Marina A. Dominguez-Steglich*†, Silvana Guioli, Cheni Kwok, Polly A. Weller, Milena Stevanović, Jean Weissenbach‡, Sahar Mansour*§, Ian D. Young*, Peter N. Goodfellow‖, J. David Brook*† & Alan J. Schafer

Department of Genetics, University of Cambridge, Downing Street, Cambridge CB2 3EH, UK
* Centre for Medical Genetics, City Hospital, and † Department of Genetics, Queens Medical Centre, University of Nottingham, Nottingham NG7 2UH, UK
‡ Laboratoire Généthon, 1 rue de l'Internationale, Evry 91002, France
§ Institute of Child Health, Guilford Street, London WC1N 1EH, UK

Induction of testis development in mammals requires the presence of the Y-chromosome gene *SRY*. This gene must exert its effect by interacting with other genes in the sex-determination pathway. Cloning of a translocation chromosome breakpoint from a sex-reversed patient with campomelic dysplasia, followed by mutation analysis of an adjacent gene, indicates that *SOX9*, an *SRY*-related gene, is involved in both bone formation and control of testis development.

THE *SRY* (*sex-determining region Y*) gene is a dominant inducer of testis development in mammals[1–3]. The SRY protein contains a DNA-binding motif, termed an HMG box, which is present in several transcription factors. The SRY HMG box binds to specific DNA sequences, suggesting that it affects transcription of genes 'downstream' in the testis development pathway. Since the discovery of *SRY*, many other genes have been identified that encode proteins with related HMG boxes[3]. Those that encode proteins with more than 60% similarity to the *SRY* HMG box region have been termed *SOX* genes.

The identification and cloning of *SRY* depended on the investigation of the genomes of patients with sex reversal syndromes, some with chromosomal rearrangements. In addition to *SRY*, several autosomal and one X-linked loci have also been linked with the failure to develop a testis[4–9]. Duplications of the X chromosome short arm cause XY female development[4]. The sex reversal in these patients results from the presence of two active copies of *DSS* (dosage-sensitive sex-reversal gene) which maps to a 160-kilobase (kb) region of Xp21 (ref. 8). Autosomal loci on chromosome 9p and on 10q have been implicated by chromosomal deletions in XY females[6,7]. It is not known if the sex reversal in these instances is due to monosomy for dosage-sensitive genes or whether the deletions reveal recessive mutations. A third autosomal locus, *SRA1*, is on chromosome 17 (ref. 10) and, in this case, the sex reversal is associated with campomelic dysplasia (CD), a skeletal malformation syndrome. The most obvious feature of CD is congenital bowing and angulation of the long bones which is often found combined with other skeletal abnormalities and defects of cartilage formation[11]. Patients usually die in the first months of life from respiratory failure, but the severity of the phenotype is variable and a few patients survive into adult life. So far there have been at least 121 reported cases of CD. Of those that have been karyotyped, 24 are 46,XX females, 14 are 46,XY males, 36 are 46,XY females, with a gradation of genital defects[10,12,13]. The remaining 47 non-karyotyped cases show a skewed sex ratio of 31:16 in favour of females. Some of the sex-reversed cases examined histologically exhibit gonadal dysgenesis, implying that the gene(s) responsible for CD also plays a part in testis formation.

The inheritance pattern of CD is not obvious. Many reviewers have concluded that autosomal recessive inheritance is likely[14], although it is difficult to distinguish this pattern from autosomal dominant inheritance with variable penetrance. Similarly, it is not clear whether the bone malformation and sex reversal are caused by mutation of a single gene or of a pair of linked genes in a contiguous gene syndrome. Five chromosomal rearrangements associated with CD and sex reversal have been reported that localize the gene(s) responsible to the long arm of human chromosome 17 (refs 10, 12, 15). This localization has been refined to 17q24.1–q25.1 with *GH* and *TK* as flanking markers[10]. We have constructed a high-resolution map across this 20-megabase (Mb) region using a panel of whole-genome radiation hybrids. The map has been used to position the translocation breakpoint from a 46,XY,t(2;17) (q35;q23–24) sex-reversed CD individual (patient E.)[12]. We have found an *SRY*-related gene, *SOX9*, adjacent to the translocation breakpoint. Mutation analysis and DNA sequencing have been used to demonstrate that both CD and sex reversal can be caused by mutations in *SOX9*.

High-resolution map of 17q24.1–q25.1

Radiation hybrid mapping allows the integration of different types of markers into a single map[16,17]. We used the polymerase chain reaction (PCR) to screen DNA samples from a panel of 129 whole-genome-radiation fusion hybrids, with a total of 38 markers across the region from *GH* to *TK* on chromosome 17. The same markers were then tested on the somatic cell hybrid B1, which was constructed by fusing mouse L cells with fibroblasts from patient E., a sex-reversed CD patient. The hybrid B1 retains the human translocation chromosome 2pter–q35:17q23–qter in the absence of the normal human chromosome 17 and of the reciprocal translocation chromosome. Chromosome 17 markers present in B1 must be located distal to the breakpoint (that is, between the breakpoint and the end of the long arm of chromosome 17), whereas markers missing from the hybrid must be located proximal to the breakpoint. From this analysis, we deduced that the microsatellite marker *D17S970* was the

‖ To whom correspondence should be addressed.

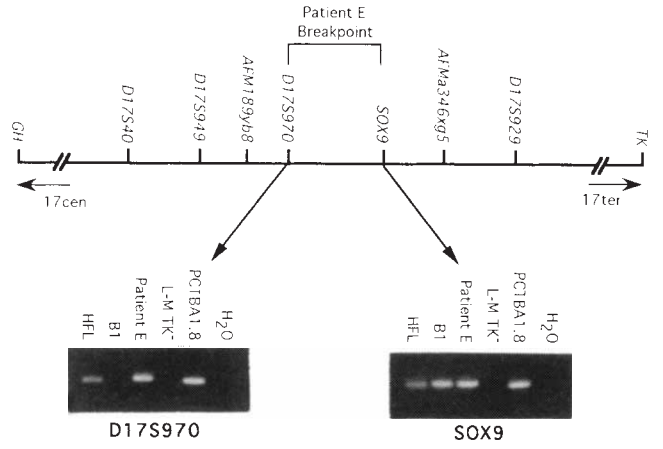

FIG. 1 Radiation hybrid map of 17q across the translocation breakpoint in patient E. STS markers are written vertically above a solid bar representing genomic DNA. The markers flanking the translocation breakpoint are indicated. Below, flanking STS markers *D17S970* and *SOX9* tested on the B1 hybrid by PCR showing their absence/presence respectively. B1 is an L-M TK⁻ somatic cell hybrid containing the translocation chromosome 2pter–q35:17q23–qter from patient E. PCTBA1.8 is a mouse somatic cell hybrid containing human chromosome 17 only; HFL is a human fibroblast; L-M TK⁻ is a mouse fibroblast.
METHODS. The whole-genome-irradiation and fusion hybrids (WG-RH) were constructed by fusing A23 hamster fibroblasts with irradiated (6,000 rads) HFL human fibroblasts[17]. The STS order was determined using the RHMAP programmes[42]. PCR reactions were performed with 50 ng genomic DNA, 1.5 mM $MgCl_2$ (2.5 mM $MgCl_2$ for *SOX9* primers), 50 mM KCl, 0.1% Triton-X100, 10 mM Tris-Cl (pH 8.5), 1.5 U *Taq* polymerase and 1 μM each primer. Thermocycling parameters were 94 °C for 60 s, followed by 35 cycles of 94 °C for 30 s; 55 °C for 30 s; 72 °C for 60 s, then 5 min at 72 °C. The presence or absence of each STS in each WG-RH was determined by electrophoresis through ethidium bromide stained agarose gels. Primer sequences: AFMa346xg5-A, 5′-CCAAAGTCCTAAAGGTGGG-3′; AFMa346xg5-B, 5′-TTTCAGGCAAATAAGGCAG-3′; AFM189yb8-A, 5′-TGGCAATCTAACAGATGAGA-3′; AFM189-yb8-B, 5′-TCNCAAATGTCATATATCCA-3′; SOX9-A, 5′-AGTCCAGATTGACTGGAACACA-3′; SOX9-B, 5′-GCAATAAGATACTAATATGTAGAG-3′ D17-S40-A, 5′-GTCAGCAGAAATCCTAAAGG-3′; D17S40-B, 5′-GACTAATGCCGATGGTTAAG-3′. The other primer sequences are available through the Genome Data Base.

closest proximal marker to the breakpoint and the gene *SOX9* was the flanking distal marker (Fig. 1). Assuming a distance of ~20 Mb between *GH* and *TK*, the radiation hybrid map can be used to estimate the distance between *D17S970* and *SOX9* as 1–2 Mb.

Translocation breakpoint localized

The markers flanking the translocation breakpoint were used to screen the ICRF[18] and CEPH YAC libraries[19] and a YAC contig was constructed based on STS content (Fig. 2). Probes from the ends of the YACs were isolated and tested back on hybrid B1 DNA as well as the other YACs to verify the contig. The YAC ICRFy900D0292, which was identified by the *SOX9* probe, yielded an end clone, D0292-R, that failed to hybridize with hybrid B1 DNA. This result placed the translocation breakpoint in the region between *SOX9* and D0292-R. Analysis of ICRFy900D0292 by pulsed-field gel electrophoresis showed that these markers were separated by 105–120 kb (data not shown).

A cosmid contig of the region between *SOX9* and D0292-R was constructed by screening the ICRF chromosome 17 cosmid library[18] with inter-Alu PCR products derived from one of the YACs (946 E12) that spans the region. Inter-Alu positive cosmids were tested with markers flanking the translocation breakpoint, and these served as starting points for a cosmid walk. A contig was assembled using isolated cosmid ends to identify overlapping cosmids from the YAC Alu-PCR positive cosmid set (Fig. 2). The end clones were mapped back onto the hybrid B1, and one of these detected the breakpoint in patient E. and hybrid B1 on Southern blots of *Bam*HI-digested DNA (data not shown). The distance from the breakpoint to the *SOX9* open reading frame is 88 kb.

Characterization of the *SOX9* gene

Transcripts corresponding to the human *SOX9* gene were isolated previously by screening a testis complementary DNA library at high stringency with a *SOXA* HMG-box probe[20]. The isolated cDNAs were identified as *SOX9* based on similarity to the published partial sequence containing the mouse *Sox-9* HMG box region[21]. We have assembled a composite transcript of 3,934 base pairs (bp) using sequence obtained from cDNA clones isolated from three independent libraries (Fig. 3*a*). Comparison of this sequence with the corresponding genomic DNA revealed the presence of two introns (Fig. 3*a*, *b*), the boundaries of which have canonical splice site junctions. *SOX9* is the first *SOX* gene reported to contain introns; other *SOX* genes studied at the genomic level are single exon genes[1,20,22,23]. The 3′ region of the composite cDNA sequence contains a potential polyadenylation signal located 19 bp upstream from a terminal polyadenosine tract. The cDNA sequence diverges from the genomic sequence at the poly(A) tract, indicating that the cloned cDNA contains the 3′ end of the *SOX9* transcript. The composite cDNA contains an open reading frame (ORF) with an HMG box and four potential start codons. Using the most 5′ methionine as the translation start site, a polypeptide of 509 amino acids is predicted (Fig. 3*a*). This methionine is located 125 bp downstream of an in-frame stop codon, strongly suggesting that the complete ORF is contained within the cloned cDNA sequences. Northern blot analysis using a *SOX9* cDNA probe detects a transcript of ~4.5 kb in total cytoplasmic RNA from adult testis, adult heart and fetal brain (data not shown). The SOX9 protein HMG box domain at amino acids 104–182 shares 71% similarity with the SRY HMG box and the C-terminal third of the protein has a proline- and glutamine-rich region, similar to activation domains present in some transcription factors[24]. DNA and protein sequence database searches and subsequent sequence alignment with the *SOX9* HMG box identified mouse *Sox-9*, *Sox-8* and *Sox-10* as the most related sequences at 100, 98 and 93% predicted amino-acid identity, respectively. The same searches using sequences located outside the HMG box did not detect any significant matches in the databases.

Initial localization of *SOX9* using a monochromosomal somatic cell hybrid mapping panel, followed by sublocalization using chromosome-17 deletion hybrids mapped the gene to 17q23-qter (Fig. 3 legend). This localization was refined to 17q24 by fluorescence *in situ* hybridization.

Mutation analysis of *SOX9*

The juxtaposition of *SOX9* and the translocation breakpoint in patient E. prompted us to test for mutations in this gene in DNA samples from patients with clinically confirmed CD. Initial screening was performed using a single-strand conformation polymorphism (SSCP) assay. Primers were designed to amplify the known coding sequences and intron/exon junctions in overlapping fragments of ~150 bp. Fragments that gave altered SSCP patterns (unique SSCP conformers) were cloned into plasmid vectors and sequenced. Nine patient samples were investigated; these samples yielded six heterozygous mutations. We now describe three patients in detail.

Patient S.H. (46,XX female) (ECACC no. DD1813). This patient was delivered at term with typical features of CD: micrognathia, hypoplastic scapulae, bilateral talipes equinovarus, hypoplastic cervical vertebrae, bowing of the long bones, and eleven pairs of ribs. Cloning and sequencing of a unique *SOX9* SSCP conformer for this individual revealed a cytidine-to-thymidine base transition (nucleotide 583) which introduces a stop codon at amino-acid position 195 of the predicted 509-

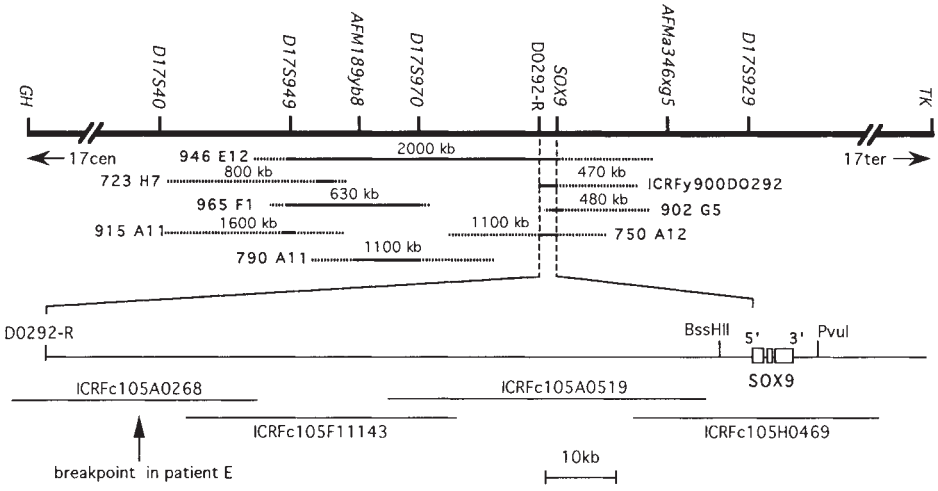

FIG. 2 Relationship between the chromosome-17 radiation hybrid map, YAC contig and cosmid contig for the region of the Patient E. translocation breakpoint. Markers are indicated vertically above a solid bar representing genomic DNA. YACs are positioned below: solid bars indicate confirmed marker content, dashed lines represent the possible extent of the YAC. Sizes indicated are for the entire YAC and may include non-chromosome 17 sequences present as a result of chimaerism. The STS markers *D17S970* and *D17S949* had already been used to screen the CEPH library as part of the Genethon and Whitehead/MIT Genome Center mapping projects. The cosmid walk is shown below an expansion of the breakpoint region genomic DNA. The organization and orientation of *SOX9* are indicated. ICRF Reference Library YAC and cosmids[18] are indicated as such, all other YACs are from Centre d'Etude du Polymorphisme Humain[19].
METHODS. YAC and cosmid ends were isolated by vectorette PCR[43] using the published YAC primers and cosmid vector (Lawrist4) primers LAW4L: CGCCTCGAGGTGGCTTATCG and LAW4R: ATCATACACATACGATTTAGGTGAC.

amino-acid sequence (Fig. 4). Both parents of this patient were screened by SSCP for this portion of *SOX9* and neither showed an aberrant shift (Fig. 4). In addition, DNA samples from over 100 unaffected individuals were screened by SSCP for this region of *SOX9*. No anomalous shifts were seen in any normal individual. This is a *de novo* mutation.

Patient A.H. (46,XY female) (NIGMS no. GM01737). This sex-reversed individual was delivered at term with a full spectrum of CD symptoms, including short bowed limbs, small scapulae and characteristic facial features[25]. Normal external female genitalia were present and the gonads were poorly differentiated with a substantial number of germ cells. Cloning and sequencing of the unique SSCP conformer for this patient (Fig. 4) identified a single G insertion in a series of six Gs (nucleotides 783–788) contained within codons 261–263 of *SOX9*. The resulting frameshift introduces a premature stop codon such that a 294-amino-acid truncated protein would be translated. Parental DNA of this patient could not be obtained. To investigate the possibility that this mutation occurs in unaffected individuals, SSCP was performed on this region of *SOX9* in more than 100 individuals without CD. No shifts corresponding to the patient A.H. unique conformer were found.

Patient G. (46,XY female). Following ultrasound findings of short limbs and cystic hygroma, this fetus was aborted at 17 weeks. Clinical and radiological features include micrognathia, bowing of the limbs, hypoplastic scapulae, dislocated hips and eleven pairs of ribs. Normal female genitalia were present and the ovaries appear histologically normal with oocytes. The mutation found in the unique SSCP conformer from this patient is the result of a 4-bp insertion following amino-acid 286 (nucleotide 858) of the predicted protein sequence (Fig. 4). This frameshift introduces a premature stop at the same position as in patient A.H. SSCP analysis of this region of *SOX9* from both parents revealed a normal *SOX9* shift (Fig. 4). This is a *de novo* mutation.

Mutations identified in the other three CD patients include a transition in the splice acceptor consensus dinucleotide in an XY female patient and transitions causing two different amino-acid substitutions in an XY male and an XX female.

Discussion

We have used a positional cloning strategy to define a breakpoint from a patient with both CD and autosomal XY sex reversal. The open reading frame of *SOX9*, an *SRY*-related gene, is located 88 kb distal to the breakpoint on chromosome 17. We have found mutations in single alleles of *SOX9* in six of nine campomelic dysplasia patients examined. The three mutations described in detail here would be expected to destroy gene function: two mutations cause frameshifts that lead to premature chain termination and loss of one third of the protein, and one mutation causes a premature termination that truncates the protein at 40% of its predicted length. SSCP analysis of both parents of two of the patients revealed the absence of the mutation present in their offspring. The *de novo* appearance of a mutation in a sex-reversed CD patient establishes that alterations in *SOX9* can cause both CD and autosomal sex reversal.

The precise relationship between the translocation breakpoint and *SOX9* is at present unclear. The *SOX9* transcript in adult testis, adult heart and fetal brain is ~4.5 kb, but the isolated cDNAs correspond to 3.9 kb of the transcript, leaving ~600 bp of untranslated sequence unaccounted for. The genomic arrangement of *SOX9* is such that the 5′ end is oriented towards the chromosome-17 centromere and closest to the breakpoint. It is possible that one or more exons are present 5′ to the known exons, and that these are disrupted by the translocation. Alternatively, the translocation may disrupt expression by a more subtle mechanism[26–28]. It is striking that several of the CD translocation patients have survived early childhood and the disease may be milder in these individuals[29].

Campomelic dysplasia has been described as an autosomal recessive or even X-linked disease, although a few cases are more consistent with a dominant disorder[30–32]. Our results support the suggestion that CD is an autosomal dominant disease. We have not detected mutations in both *SOX9* alleles of any patient, in spite of having performed SSCP across >70% of the open reading frame. The predicted loss of gene function in these mutants, together with the absence of mutations in both alleles implies that the dominance is due to haplo-insufficiency rather than gain of function. Dosage sensitivity is often a feature of regulatory genes and has been described for several sex determination systems, including the mammalian pathway[8,33].

A prediction for autosomal dominance of *SOX9* mutations is that deletions resulting in monosomy of 17q should cause CD. Such deletions are very rare, presumably because of an associated lethality, and have nearly always been reported associated with a ring chromosome. Interestingly, in a single reported 17q deletion not associated with a ring chromosome, the patient exhibited a number of physical features that occur in CD, including angulation of the lower limbs[34]. Cases diagnosed as CD have a wide range and severity of associated phenotypes, including 'acampomelic' CD and the suggestion of long-bone and short-

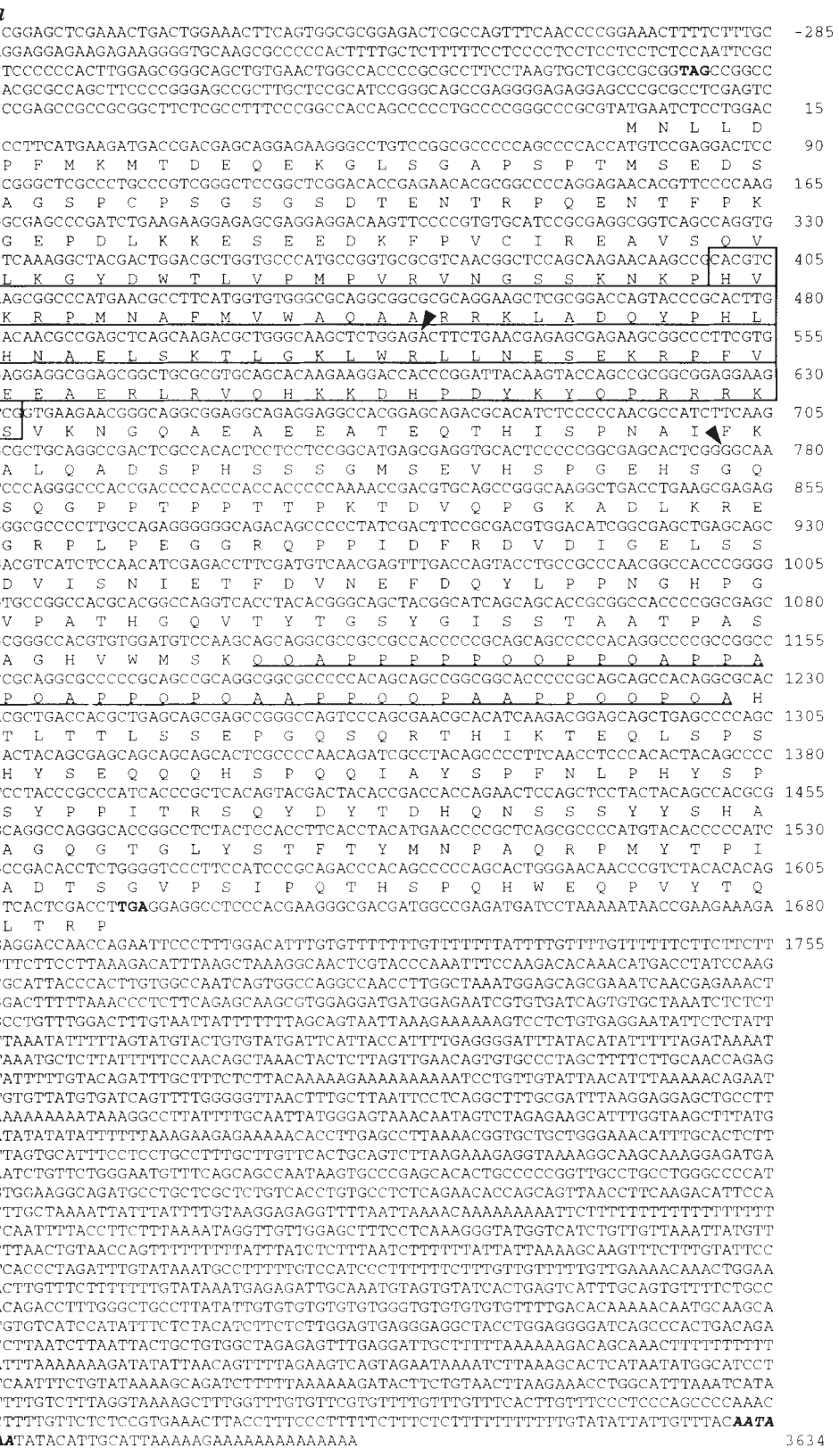

FIG. 3 *a*, Nucleotide and predicted amino-acid sequence of *SOX9*. Numbering is with respect to the A in the first methionine codon of the open reading frame. An in-frame 5′ stop codon and the predicted termination stop codon are in bold. The HMG box is boxed and the proline- and glutamine-rich region is underlined. The locations of the introns are indicated with arrows and a potential polyadenylation signal is indicated by bold italic letters. *b*, Genomic organization of the *SOX9* gene. The solid bar represents genomic DNA. The *SOX9* exons are boxed and the HMG box cross-hatched. E, *Eco*RI. Below, the cDNA is represented as an open box with the HMG box cross-hatched. The positions of the introns are indicated.

METHODS. Initial cDNA clones were obtained by screening a λgt11 human testis library (Clontech) using a *SOXA* box probe[20]. A composite transcript was determined from these overlapping clones and from further clones obtained from an HT1080 (fibrosarcoma) cDNA library (gift from D. L. Simmons) and a human fetal brain library (HGMP Resource Centre, Harrow). Sequencing was performed using the dideoxy chain termination method. The location of the intron/exon boundaries was determined by restriction mapping of genomic and cDNA clones and by comparison of the genomic and cDNA sequences. Initial localization of the *SOX9* cDNA to chromosome 17 was determined by probing a somatic cell hybrid panel. Sublocalization to 17q23–qter was determined using a panel of chromosome-17 deletion hybrids, including PCTBA1.8, TRID62, PLT8, PJT2A1 and DCR1 (ref. 44), and refined to 17q24 by fluorescence *in situ* hybridization to normal human metaphase spreads.

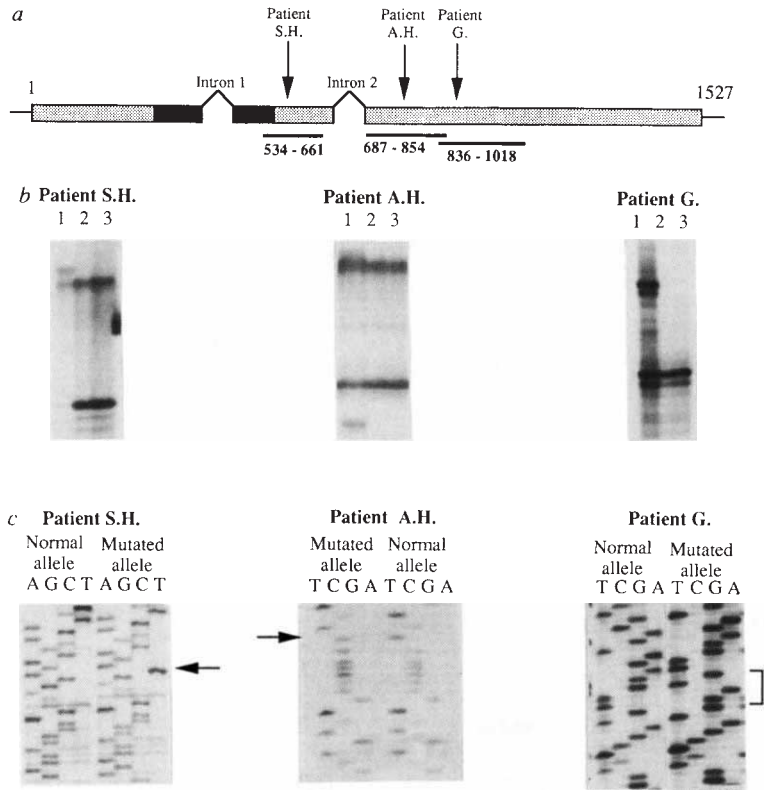

FIG. 4 Single-strand conformation polymorphism (SSCP) and sequence analysis of *SOX9* in campomelic dysplasia patients. *a*, *SOX9* open reading frame (shaded boxes) showing the HMG box (heavy shading). Numbers indicate nucleotide sequence beginning with the A of the first methionine, with introns occurring after nucleotides 431 and 685. Solid bars below indicate regions of the ORF generating unique SSCP conformers. Positions of mutations are indicated by arrows. *b*, SSCP using primers indicated in *a*. Lane 1, patient DNA. For patients S.H. and G., lanes 2 and 3 are DNAs from father and mother, respectively. For patient A.H., lanes 2 and 3 are DNAs from unrelated (normal) individuals. *c*, Sequencing gels of normal and mutated patient alleles. The position of each mutation is indicated. Sequence for patients S.H. and A.H. is that of the coding strand; for patient G., the sequence is of the non-coding strand.

METHODS. Primer sequences: 534, 5′-GAGGAAGTCGGTGAAGAAC-3′; 661, 5′-TCGCTCATGCCGGAGGAGGAG-3′; 687, 5′-GCAATCCCAGGGCCCACCGAC-3′; 854, 5′-TTGGAGATGACGTCGCTGCTC-3′; 836, 5′-GCAGCGACGTCATCTCCAAC-3′; 1018, 5′-GCTGCTTGGACATCCACACGT-3′. PCRs (10 μl) were performed as for Fig. 1, with the non-radioactive dCTP concentration reduced to 1/10 and the addition of 0.05 μl [α-^{33}P]dCTP (1,000–3,000 Ci mmol^{-1}, 10 mCi ml^{-1}) and 0.2 μM of each primer. Reactions were cycled for 30 s at 94 °C, 30 s at 65 °C (534–661 and 836–1,018) or 70 °C (687–854), 45 s at 72 °C for 35 cycles. PCR products were denatured by adding 10 μl 0.2% SDS, 20 mM EDTA then 10 μl 95% formamide, 20 mM EDTA, 0.05% bromophenol blue, 0.05% xylene cyanol and heating to 100 °C for 5 min. 2 μl were loaded onto 6% acrylamide : bisacrylamide (37.5 : 1), 5% glycerol gels. Electrophoresis was carried out at 25 W at 4 °C. PCR products from duplicate reactions were subcloned and at least 10 clones from each were sequenced by either the dideoxy chain termination method or by DyeDeoxy Terminator Cycle Sequencing (ABI). DNA profiling of each family using 12 chromosome-8 microsatellite markers (heterozygosity >70%) showed no discordant results between parents and offspring.

bone varieties[11]. It will be of interest to determine the extent of *SOX9* involvement in all cases diagnosed as CD.

By analogy with *SRY*, it has been suggested that *SOX* genes might act as transcription factors in developmental control pathways. Some *SOX* proteins show sequence-specific binding[35–37] and the C-terminal third of the SOX9 protein has a proline- and glutamine-rich region, similar to activation domains present in some transcription factors[24]. This region would be missing in products translated from the mutated sequences present in the patients described here.

SOX9 is not the first mammalian gene to be shown to have a dosage-sensitive role in sex determination. *DSS* causes male-to-female sex reversal, with varying degrees of masculinization, when present in two copies in 46,XY individuals. Absence of *DSS* is compatible with male development in the presence of *SRY*, but it is not known if it is compatible with female development in 46,XX individuals. Because of the importance of *SOX9* in bone formation, it is likely that nullisomy for *SOX9* is lethal. *SOX9* monosomy is compatible with ovarian development[34] and trisomy for 17q, including the region containing *SOX9*, has not been associated with sex reversal[38]. The cause of the variability of sex reversal associated with CD remains to be determined. There is no obvious correlation between the severity of the skeletal anomalies and the incidence of sex reversal[29]. The presence or absence of sex reversal in XY individuals may be determined by the nature of the mutation, or could lie in allelic differences at other loci.

The dosage sensitivity of *SOX9* in sex determination and its sequence similarity to *SRY* suggest a possible evolutionary relationship between the two genes. It is plausible that a primordial dosage-dependent sex-determination system evolved into a dominant induction system by alteration of *SOX9* or another *SOX* gene[39]. The mutated gene could function as a dominant inducer by becoming constitutively expressed and thus, when present, increasing dosage to be above a threshold required for male development.

There is a large body of indirect evidence suggesting that the sex-determining function of *SRY* is expressed in pre-Sertoli cells in the developing gonadal ridge[3]. *SOX9* could be required in these cells, and *SRY* and *SOX9* interactions may be required for full cell function. Another possibility is that *SOX9* expression is required in a cell type that interacts with *SRY*-expressing pre-Sertoli cells to form testis. It is known that mesenchymal cells migrate from the mesonephros underlying the genital ridge and that these migratory cells are required for testis formation[40]. Mesenchymal cells give rise to both bone and cartilage forming cells[41] and this might provide the link between CD and sex reversal. The identification of *SOX9* as a gene mutated in both CD and autosomal sex reversal provides new tools for studying bone formation and sex determination. □

Received 3 October; accepted 14 November 1994.

1. Sinclair, A. H. *et al. Nature* **346,** 240–244 (1990).
2. Koopman, P., Gubbay, J., Vivian, N., Goodfellow, P. & Lovell-Badge, R. *Nature* **351,** 117–121 (1991).
3. Goodfellow, P. N. & Lovell-Badge, R. *A. Rev. Genet.* **27,** 71–92 (1993).
4. Bernstein, R. *et al. J. med. Genet.* **17,** 291–300 (1980).
5. Pelletier, J. *et al. Nature* **353,** 431–434 (1991).
6. Bennett, C. P. *et al. J. med. Genet.* **30,** 518–520 (1993).
7. Wilkie, A. O. M. *et al. Am. J. med. Genet.* **46,** 597–600 (1993).
8. Bardoni, B. *et al. Nature Genet.* **7,** 497–501 (1994).
9. Luo, X., Ikeda, Y. & Parker, K. L. *Cell* **77,** 481–490 (1994).
10. Tommerup, N. *et al. Nature Genet.* **4,** 170–174 (1993).
11. McKusick, V. A. *Mendelian Inheritance in Man* (The Johns Hopkins Press, Baltimore, 1992).
12. Young, I. D., Zuccollo, J. M., Maltby, E. L. & Broderick, N. J. *J. med. Genet.* **29,** 251–252 (1992).
13. Houston, C. S. *et al. Am. J. med. Genet.* **15,** 3–28 (1983).
14. Cremin, B. J., Orsmond, G. & Beighton, P. *Lancet* **i,** 488–489 (1973).
15. Maraia, R., Saal, H. M. & Wangsa, D. *Clin. Genet.* **39,** 401–408 (1991).
16. Walter, M. A. & Goodfellow, P. N. *Trends Genet.* **9,** 352–356 (1993).
17. Walter, M. A., Spillet, D. J., Thomas, P., Weissenbach, J. & Goodfellow, P. N. *Nature Genet.* **7,** 22–28 (1994).
18. Lehrach, H. *et al.* in *Genome Analysis 1: Genetic and Physical Mapping* (eds Davies, K. E. & Tilghman, S. H.) 39–81 (Cold Spring Harbor Laboratory Press, New York, 1990).

19. Cohen, D., Chumakov, I. & Weissenbach, J. *Nature* **366,** 698–701 (1993).
20. Stevanovic, M., Lovell-Badge, R., Collignon, J. & Goodfellow, P. N. *Hum. molec. Genet.* **2,** 2013–2018 (1993).
21. Wright, E. M., Snopek, B. & Koopman, P. *Nucleic Acids Res.* **21,** 744 (1993).
22. Farr, C. J. *et al. Mamm. Genome* **4,** 577–584 (1993).
23. Schilham, M. W., van Eijk, M., van de Wetering, M. & Clevers, H. C. *Nucleic Acids Res.* **21,** 2009 (1993).
24. Mitchell, P. J. & Tjian, R. *Science* **245,** 371–378 (1989).
25. Hoefnagel, D., Wurster-Hill, D. H., Dupree, W. B., Benirschke, K. & Fuid, G. L. *Clin. Genet.* **13,** 489–499 (1978).
26. Dillon, N. & Grosveld, F. *Curr. Opin. Genet. Dev.* **5,** 260–264 (1994).
27. Capel, B. *et al. Nature Genet.* **5,** 301–307 (1993).
28. Tommerup, N. *J. med. Genet.* **30,** 713–727 (1993).
29. Mansour, S. thesis, Univ. London (1994).
30. Bianchine, J. W., Risemberg, H. M., Kanderian, S. S. & Harrison, H. E. *Lancet* **I,** 1017–1018 (1971).
31. Thurmon, T. F., DeFraites, B. S. & Anderson, E. E. *J. Pediatr.* **83,** 841–843 (1973).
32. Lynch, S. A., Gaunt, M. L. & Minford, A. M. *J. med. Genet.* **30,** 683–686 (1993).
33. Parkhurst, S. M. & Meneely, P. M. *Science* **264,** 924–932 (1994).
34. Bridge, J. *et al. Am. J. med. Genet.* **21,** 225–229 (1985).
35. Harley, V. R. *et al. Science* **255,** 453–456 (1992).
36. Denny, P., Swift, S., Connor, F. & Ashworth, A. *EMBO J.* **11,** 3705–3712 (1992).
37. van de Wetering, M., Oosterwegel, M., van Norren, K. & Clevers, H. *EMBO J.* **12,** 3847–3854 (1993).
38. Lenzini, E. *et al. Ann. Genet.* **31,** 175–180 (1988).
39. Foster, J. W. & Graves, J. A. *Proc. natn. Acad. Sci. U.S.A.* **91,** 1927–1931 (1994).
40. Buehr, M., Gu, S. & McLaren, A. *Development* **117,** 273–281 (1993).
41. Wheater, P. R., Burkitt, H. G. & Daniels, V. G. *Functional Histology* (Churchill Livingstone, Edinburgh, 1979).
42. Boehnke, M., Lange, K. & Cox, D. R. *Am. J. hum. Genet.* **49,** 1174–1188 (1991).
43. Riley, J. *et al. Nucleic Acids Res.* **18,** 2887–2890 (1990).
44. Black, D. M., Nicolai, H., Borrow, J. & Solomon, E. *Am. J. hum. Genet.* **52,** 702–710 (1993).

ACKNOWLEDGEMENTS. J.W.F., M.A.D.-S. and S.G. contributed equally to this work. We thank E. Hatchwell, S. Youings, N. Dennis, D. Donnai, C. Garrett, C. Hall, I. Moore, R. Mueller, R. Scott, J. Tolmie and R. Winter for patient samples and clinical details; H. Lehrach, H. Hummerich, D. L. Simmons, I. Kerr and the HGMP Resource Centre for libraries and clones; E. Solomon for hybrid DNAs; R. Critcher, P. Thomas and E. Rossi for *in situ* hybridizations; S. Marc and G. Casey for help in obtaining markers; G. Camerino and R. Lovell-Badge for discussion; D. Spillett and M. Walter for radiation hybrids; and P. Koopman and E. Wright for communication of results before publication and for discussion. This work was supported by the Wellcome Trust (J.W.F., P.A.W., A.J.S., P.N.G.), a Human Frontier Science Programme Organization Fellowship (M.A.D.-S.), the Medical Research Council (P.N.G.), the European Community (J.W., P.N.G.), the European Community SCIENCE Programme (S.G.), the University of Nottingham Medical School (J.D.B.), and a Peterhouse Research Studentship (C.K.).

A high-resolution image of atomic hydrogen in the M81 group of galaxies

M. S. Yun*†, P. T. P. Ho* & K. Y. Lo‡

* Harvard-Smithsonian Center for Astrophysics, 60 Garden Street, Cambridge, Massachusetts 02138, USA
† California Institute of Technology, Robinson 105-24, Pasadena, California 91125, USA
‡ Astronomy Department, University of Illinois, Urbana, Illinois 61801, USA

It has long been recognized that interactions between galaxies are important in determining their evolution. The distribution of gas—out of which new stars are formed—is strongly affected; in particular, gas may be concentrated near the nucleus, leading to a burst of star formation[1–4]. Here we present a map of atomic hydrogen (H I) in the nearest interacting group of galaxies (that dominated by M81), obtained by combining 12 separate fields observed with the Very Large Array. The H I that surrounds M81, M82 and NGC3077 (the most prominent galaxies in the group) is dominated by filamentary structures, clearly demonstrating the violent disruption of this system by tidal interactions. These observations should have detected all H I complexes more massive than 10^6 solar masses, meaning that our map contains all structures that might evolve into new dwarf galaxies.

With the Very Large Array (VLA) in the most compact D configuration, four fields centred around M82 were observed (3 h per field) on 24 and 25 January 1990, and eight additional fields including M81 and NGC3077 were observed (2 h per field) on 29 April and 1 May 1991, using all 27 telescopes. The achieved angular resolution of ~1 arcmin corresponds to a resolution of ~1 kpc at the systemic distance of 3.6 Mpc (ref. 5). Quasars 3C48 and 3C286 were used to set the flux-density scale and to calibrate the instrumental response across the bandpass of 5.125 MHz. The VLA calibrator 0831 + 557 was also observed to calibrate short-term variations of the system performance. With a spectral resolution of 48.8 kHz (10.3 km s^{-1}), we covered the full velocity range (~600 km s^{-1}) of the entire map by shifting the centre of our spectral window accordingly.

Figure 1 shows the H I distribution in the M81 group; this H I image of the 150 kpc region is at 1-kpc spatial resolution. The comparison of the H I and the optical images shows that although this system is a favourite testing ground for the density-wave theory and disk dynamics[6], active Seyfert nuclei[7,8], as well as starburst activities[9], little sign of tidal interactions can be seen in the optical image. Previous H I studies have suggested tidal interactions[10–17]. The remarkable result here is the extensive array of filamentary tidal features threading all three galaxies, dominating the H I distribution. Each galaxy has a concentration of gas surrounding it, with the 'south tidal bridge' connecting M81 and NGC3077, and the 'north tidal bridge' connecting NGC3077 and M82. This is the first time that the north tidal bridge is traced in its full extent. The physical properties of the main H I features are summarized in Table 1. We will now discuss our observations of the various features found in the H I and optical maps.

TABLE 1 Observed properties for the main H I features of the M81 group

Feature	N_{HI} (10^{21} cm^{-2})	M_{HI} ($10^9 M_\odot$)	M_{HI}(ADS) ($10^9 M_\odot$)	ΔV (km s^{-1})
M81	10.6 ± 0.2	2.63 ± 0.52	2.19 ± 0.22	30–45
M82	10.3 ± 0.2	0.75 ± 0.15	0.72 ± 0.07	40–140
NGC3077	10.7 ± 0.2	0.65 ± 0.13	1.00 ± 0.10	30–40
Concentration I	7.8 ± 0.2	0.29 ± 0.06	0.20 ± 0.05*	45–100
Concentration II	5.1 ± 0.2	0.24 ± 0.05	—	25–30†
South tidal bridge	2.4 ± 0.2	0.24 ± 0.05	—	10–30
North tidal bridge	1.6 ± 0.2	0.19 ± 0.04	—	20–30

Symbols used: N_{HI}, H I column density; M_{HI}, total H I mass; M_{HI}(ADS), total H I mass within the Holmberg radius measured with a 76-m telescope (angular resolution $\theta \approx 4$ arcmin) by Appleton, Davies and Stephenson[15]; ΔV, linewidth, full-width at half-maximum.
* H I mass estimated for Ho IX by Appleton, Davies and Stephenson[15].
† Two separate velocity components seen, each with $\Delta V \approx 25$–30 km s^{-1} (80–140 km s^{-1}, full-width at zero intensity).

M81. In the optical image, M81 appears to be a two-arm spiral. In the inner disk, the H I spiral arms trace the optical arms very closely. Moving beyond the optical disk, more H I arms can be seen which appear to be less tightly wound. West of the nucleus, one of the H I arms appears to wrap around to the east connecting with concentration I. East of the nucleus, two H I arms seem to continue on as two long spirals over 180° in angular extent, with the inner one continuing onto the south tidal bridge. The H I kinematics are shown in Fig. 2. Within the central 20 arcmin (20 kpc) around M81, the kinematics (the regular spider-like pattern for the isovelocity contours) show circular rotation. That the contours become progressively further apart away from the nucleus, shows differential rather than rigid-body rotation, that is, rotation is slower further out. This drop-off in circular rotation velocity with radius, also known as a rotation curve, was studied by Kent[18]. He found that the mass of the large bulge and the disk alone is sufficient to reproduce the observed rotation out to a radius R of 20 kpc (the only system in his sample of 16